Rational-RC Technical Report: Governing Formulations

Mechanism-based probabilistic formulations for deterioration modules

Scope: This technical note summarizes the governing equations used in the Rational-RC framework. The implementation details are referenced to the code repository.

1 Formulation of modules

1.1 Membrane module

The deterioration of waterproof membranes is highly complex. Factors such as chemical composition, constructio, in-service stress, moisture exposure, temperature, and overlay condition all influence membrane aging. Due to this complexity, the material degradation mechanism is not modelled directly. Instead, a statistical approach is employed to predict the probability of membrane failure. In this formulation, the resistance is defined as the membrane service life, the load is the age in service, and the limit state is reached when the service age exceeds the service life.

The initial estimation of the service life is assumed to follow the normal distribution with a mean and standard deviation such that the product service life (life expectancy) corresponds to a 95% survival probability:

$$F(\text{product service life}) = 95\% \tag{1}$$

where F is the cumulative density function (CDF) of the service life with the known or assumed standard deviation and the mean to be solved. The probability density function (PDF) of the service life, as the derivative of CDF, can be derived.

The estimated distribution is then calibrated against field-surveyed failure rates through an optimization scheme that adjusts the standard deviation until the model solution matches observed data. This calibration accounts for the variability of in-service performance and refines the uncertainty associated with membrane deterioration. The resulting calibrated model is subsequently used for future deterioration projections, with accuracy improving as additional historical data become available.

Note: For detailed code implementation, refer to the Rational-RC software package documentation[1].

1.2 Chloride module

Chloride ions are not intrinsic to cement but may enter the pore solution of concrete through several pathways. Sources include mixing water, chloride-contaminated aggregates (e.g., sea sand), or chloride-bearing admixtures. In marine environments, reinforced concrete structures such as bridge piers in direct contact with seawater, or offshore facilities exposed to airborne sea-salt particles, are subject to continuous chloride ingress. In cold regions, the dominant source is de-icing salts, which are routinely applied to bridge decks, parking garages, and other reinforced concrete surfaces either as dry crystals or in near-saturated solutions.

Chloride in concrete may be water-soluble and insoluble. The chloride ion becomes insoluble when bonded during the hydration of $\mathrm{C_3A}$ phase to form Chloroaluminates (Friedel's salt)[2]. Chloride in the solution is soluble and does damage to the passive film of rebar. Critical chloride content is the threshold chloride content for rebar to start to depassivate or, in practical engineering, to cause noticeable corrosion damage. It is usually expressed as the mass percentage of binder or of concrete. The reported value from laboratory tests and field tests have large variance[3,4]. The variation could be attributed to many factors that affect the actual concentration of soluble chloride in the pore solution: the use of supplementary materials, water saturation level in the pore networks, and consumption of chloride-binding hydration products. For example, the carbonation of chloroaluminates releases the bound chloride into soluble chloride. Sulphate attack consumes calcium aluminate hydrates lowering the bonding capacity and further competes with chloride for bonding, releasing the bound chloride into a mobile form [2].

Despite the discrepancy in the reported critical chloride threshold value, it is widely accepted that this value depends on the pH in the concrete pore solution. It is because pH affects the stability of chloride-binding hydration products (such as calcium aluminate hydrates) and also high pH itself counteracts the depassivating effect of chloride ions. Generally, a higher critical chloride threshold value is expected for a higher pH. The $[\mathrm{Cl^-}]/[\mathrm{OH^-}]$ ratio or its nonlinear variations $[\mathrm{Cl^-}]^{\mathrm{n}}/[\mathrm{OH^-}]^{m}$, is often used as the criterion for chloride-induced depassivation of rebar [4].

In the current model, the pH condition is treated as binary (non-carbonated or carbonated). The mean critical chloride content for non-carbonated concrete is taken as 0.6% by weight of cement [5] and zero for carbonated concrete. Throughout this project, the critical chloride content is expressed as a percentage by weight of cement, since cement alkalinity is the key factor counteracting chloride effects. When converted to a percentage by weight of concrete, this value depends on the cement-to-concrete ratio.

The transport of salts in concrete can be described by the diffusion-advection equation, whereby:

$$\frac{\partial(\theta c)}{\partial t} = \nabla \cdot \left(D_{eff} \nabla \mathrm{c} + \boldsymbol{u} c\right) + \theta \left(\frac{\partial c}{\partial t}\right)_{Sink/Source} \tag{2}$$

where $c\ [kg/m^3]$ is liquid phase-averaged solute concentration, $\boldsymbol{u}\ [m/\mathrm{s}]$ is Darcy's velocity, $D_{eff}\ [m^2/\mathrm{s}]$ is effective diffusivity, term $\left(\frac{\partial c}{\partial t}\right)_{Sink/Source}$ may be introduced as chloride binding (negative) and releasing (positive) or sulphate consumption (negative). $\theta\ [-]$ is volumetric water constant.

When advection is absent, the water content remains constant, and no time-dependent chloride binding or release occurs. In this case, the governing equation simplifies to Fick's second law, which has an analytical solution. This assumption is valid below the advection zone of the concrete cover, where diffusion dominates and the water content is stable. In this treatment, the chloride source boundary is defined at the end of the advection zone and the beginning of the diffusion zone. Because the water content is constant, chloride concentration in the pore solution can be expressed as chloride content per unit weight of cement. Thus, the analytical solution applies below the convection zone.

$$C(x,t) = C_0 + (C_{S,\Delta x} - C_0) \cdot \left[1 - erf\left(\frac{a - \Delta x}{2 \cdot \sqrt{D_{app,C} \cdot t}}\right)\right] \qquad (3)$$

C_0 : initial chloride content of the concrete $[wt\!-\!.\%/cement]$

$C_{S,\Delta x}$: chloride content at a depth Δx and a time t $[wt\!-\!.\%/cement]$

Δx : depth of the convection zone (concrete layer, up to which the process of chloride penetration differs from Fick's 2nd law of diffusion) $[mm]$

$D_{app,C}$: apparent coefficient of chloride diffusion through concrete $[mm^2/year]$

erf : error function

The main challenge lies in determining the advection zone depth, Δx, and the chloride content at that depth, $C_{S,\Delta x}$. The depth of the convection zone depends on wetting and drying cycles, while the chloride content at this depth is influenced by the frequency and amount of chloride exposure. can be quantified through experimental studies or numerical simulations of chloride transport under wetting–drying conditions. The empirical quantification of these parameters can be found in the FIB model code [5] which classifies exposure conditions into two categories: "advection" (e.g., splash) and "no advection" (e.g., submerged, leakage, or spray, with $\Delta x = 0$). The boundary conditions are estimated based on the information of chloride sources such as seawater or the amount of deicing salt applied. When such information is not available, and the reinforced concrete structure is sufficiently aged in its service environment, the chloride content at a shallow depth (e.g., 12.5 mm) may be used as $C_{S,\Delta x}$ with Δx = shallow depth under no-advection assumptions. However, when advection is considered, the Δx needs to be initially determined based on the exposure conditions and the $C_{S,\Delta x}$ should be the chloride content measured at that Δx depth.

The initialized model can then be calibrated to the field chloride profile (usually at three depths: 12.5 mm, 50 mm, 100 mm). The search algorithm will find the "rapid chloride migration diffusivity" from a virtual chloride migration test, which corresponds to the apparent coefficient of chloride diffusion in concrete, $D_{app,C}$, that matches field chloride content at a given time and depths. The calibrated model employs the mean values of the rapid chloride migration diffusivity calibrated for chloride at multiple depths. The calibrated model can be further validated with the survey data at different times.

Note: Detailed implementation procedures are provided in the Rational-RC software package documentation [6].

1.3 Carbonation module

In reinforced concrete structures, carbon steel reinforcement is embedded in an alkaline environment with a pH of 12.5–13.5. This high alkalinity promotes the formation of a passive film on the steel, keeping corrosion rates extremely low. The film, however, can be destabilized either by chloride ions, even at high pH, or by carbonation, which reduces the pore solution pH to near-neutral levels (about 8.0–8.5). Once the film breaks down, the steel depassivates and can corrode at significantly higher rates. Carbonation-induced corrosion is typically uniform, with anodic and cathodic sites located in close proximity.

The carbonation process can be numerically modelled with the diffusion of CO_2 gas, its equilibrium with the dissolved species in concrete pore solution (e.g., $\mathrm{HCO_3^-}$ and $\mathrm{H_2CO_3}$), and the neutralization reaction between these carbonate and bicarbonate acid with the hydroxide ions from the hydration products such as $\mathrm{Ca(OH)_2}$ and C-S-H gel. This complex process has been modelled numerically by [7,8] with refinements to chemical interactions and porosity changes. Although such models are computationally intensive and unsuitable for probabilistic applications, they highlight key factors influencing carbonation rate. Specifically, the carbonation rate is dependent on the material properties such as $\mathrm{CO_2}$ diffusivity, and environmental factors such as the relative humidity. Empirical evidence shows that carbonation depth is approximately proportional to the square root of time, with the proportionality constant governed by material properties and exposure conditions. Systematic studies [5] have been conducted on quantifying the effects of the material properties and environmental factors on the proportional constant.

$$x_c(t) = W(t) \cdot \sqrt{2 \cdot k_e \cdot k_c \cdot (k_t \cdot R_{ACC,0}^{-1} + \epsilon_t) \cdot C_S} \cdot \sqrt{t} \tag{4}$$

$x_c(t)$: carbonation depth $[mm]$

$W(t)$: weather function $[-]$

k_e : environmental function $[-]$

k_c : execution transfer parameter $[-]$, account for curing measures

k_t : regression parameter $[-]$

$R_{ACC,0}^{-1}$: inverse effective carbonation resistance of concrete in accelerated carbonation test $[(mm^2/year)/(kg/m^3)]$

ϵ_t: error term $[-]$

C_S : CO_2 concentration $[kg/m^3]$

t : time $[year]$

Quantification of these parameters can be found in the FIB model code [5].

The Limit state for the carbonation-induced corrosion is when carbonation depth reaches the rebar surface. The probability of failure is

$$P_f = P(a - x_c < 0) \tag{5}$$

Where a is the concrete cover $[mm]$.

Whenever available, the carbonation model can be calibrated with the historical carbonation depth survey data. Calibration aligns the mean modelled carbonation depths with field observations. The calibrated parameter is the accelerated carbonation depth from a standardized test, which represents the effective carbonation resistance of concrete and is independent of ambient conditions. Predicted carbonation depths can then be validated against current or future survey data.

Note: Detailed implementation procedures are provided in the Rational-RC software package documentation [1].

1.4 Corrosion module

In the current module, corrosion is assumed to be uniform. Under this assumption, the corrosion current density, i_{corr}, which reflects the averaged section loss of the metal into the rebar surface. Rebar corrosion becomes significant when the passive film is destroyed due to carbonation, chloride ingress, or both. Once fully activated, the corrosion process can be activation-controlled, primarily governed by water content and temperature, or diffusion-limited, constrained by oxygen availability in highly saturated concrete where oxygen transport is slow.

Numerical models are capable of simulating the electrochemical process and the potential and current distribution. The coupling of the anodic and cathodic sites is modelled in a 2-D domain representing concrete cover. The activation-controlled kinetics (potential-current relationship) on the rebar is described by the Bulter-Volmer equation. The potential distribution in the concrete cover is governed by Laplace's equation. Water content and temperature affect the concrete resistivity and, therefore, the potential and current density distribution on the rebar.

The effect of temperature is specifically emphasized in a numerical model by [9], which was adopted in this project. The Arrhenius type of dependency of corrosion rate on temperature is reflected on the exchanging current density of the two half-cell reactions ($\mathrm{Fe}^{2+}/\mathrm{Fe}$ and $\mathrm{H_2O}/\mathrm{OH}^-$), and temperature-dependent resistance change between the separated anode and cathode. Although the effect of resistivity is debatable when the distribution of anodic and cathodic sites is unclear, the effect from the resistance can be tuned by the anodic/cathodic area ratio and the size of these areas, which is effectively a user-input calibration factor. A similar model was also developed by [10], and corrosion rate predictions from both models are reasonably comparable to the experimental result with varying temperature and ambient relative humidity [10,11]. The solution of the numerical model [9] has been fitted into an analytical form where i_{corr} is a function of resistivity, temperature, cover thickness and limiting current density.

$$i_{corr} = \frac{1}{\tau\rho^{\gamma}}\left[\eta T d^{\kappa} i_L^{\lambda} + \mu T \nu^{i_L^{\omega}} + \theta (T i_L)^{\nu} + X\rho^{\gamma} + \zeta\right] \tag{6}$$

where $\rho[\Omega m]$ is concrete resistivity, $T[K]$ is temperature, $d[m]$ is concrete cover thickness, $i_L[A/m^2]$ is limiting current density, and the remaining Greek symbols are fitted, unitless parameters.

It is worth mentioning that since resistivity is highly related to the water content, mathematically, one can correlate either one of them to the experimental data regardless of the physical mechanism. In the original finite element model [9], the resistivity is formulated with relative humidity. However, water content is a more preferred measure for the moisture condition in concrete because the concrete may retain a different amount of moisture depending on the pore structure and pore solution composition. Therefore, in order to use water content to replace the RH-correlated resistivity as the input, this analytical model, Equation (6) is calibrated with a resistivity-water content relationship, such that the resistivity is correlated to the water content and the model predicts the same results with the tested data at the given temperature (e.g. 25℃). An optimization algorithm was used to find such a resistivity-water content curve. The fitted analytical form of the curve can be expressed as

$$\rho = a\theta_w^b \tag{7}$$

where $\theta_w[-]$ is volumetric water content, and a, b are fitted parameters.

The limiting current density, i_L was calculated with the assumption of a Nernstian diffusion layer with a thickness δ and diffusivity D_{O_2} . The cathodic current is at equilibrium with the with mass transport.

$$i_L = zF\frac{D_{O_2}C_{s,O_2}}{\delta} \tag{8}$$

where $C_{s,O_2}[mol/m^3]$ is the amount of dissolved oxygen in a continuum; $\delta[m]$ is the effective thickness of oxygen diffusion layer; $D_{O_2}[m^2/\ s]$ is diffusion coefficient of oxygen in a continuum.

In concrete, the diffusion of oxygen takes place in both the gas phase and liquid phase. The gas and liquid bulk flow can be neglected, so the whole concrete cover is considered as the diffusion layer. The oxygen diffusion in the gas phase is much greater than the diffusion in the solution. Therefore, the gas-phase diffusion is dominant. This consideration is reasonable because the liquid phase is often discontinuous in partially saturated concrete, while gas-phase diffusion bridges these discontinuities. Therefore, the oxygen diffusion in concrete is treated with total-volume-averaging approach, where concrete is treated as a continuum, and the driving force for the oxygen diffusion is the gradient of gas mass density/concentration in the gas phase. The effective diffusivity of oxygen in concrete as a continuum should be used, as measured by typical experimental setups for diffusivity measurement [12].

Accordingly, Equation (8) can be reformulated for concrete as:

$$i_L = zF\frac{D_{e,O_2}\epsilon_g C_{g,O_2}}{d} \tag{9}$$

Where D_{e,O_2} is the effective diffusivity of oxygen in concrete, ϵ_g is the gas-phase volume fraction, C_{g,O_2} is oxygen concentration in the gas phase $[mol/m^3]$.

The effective diffusivity of oxygen in concrete, D_{e,O_2}, depends on the concrete pore structure and moisture level. It can be estimated using the empirical equation [12]:

$$D_{e,O_2} = 1.92 \times 10^{-6} \epsilon_p^{1.8} (1 - RH/100)^{2.2} \tag{10}$$

where ϵ_p is the porosity of hardened cement paste (HPC) and RH is the internal relative humidity [%]. This HCP porosity is used because diffusion along the aggregate–paste interface is considered to make up for the lack of diffusion through the aggregate particles themselves.

The porosity of hardened cement paste, ϵ_p, is related to the concrete total porosity, ϵ, by

$$\epsilon_p(t) = \epsilon(t) \left(1 + \frac{\frac{a\rho_c}{c\rho_a}}{1 + \frac{w\rho_c}{c\rho_w}} \right) \tag{11}$$

where a/c is aggregate-to-cement ratio, w/c is water-to-cement ratio, ρ_c is particle density of cement, ρ_a is particle density of aggregate (fine and coarse), ρ_w is density of water, $\epsilon(t)$ is the porosity of concrete, which changes with time with a reduction in porosity due to continuous hydration, $\Delta\epsilon_H(t)$ and carbonation, $\Delta\epsilon_c$:

$$\epsilon(t) = \epsilon_0 - \Delta\epsilon_H(t) - \Delta\epsilon_c \tag{12}$$

In this project, the porosity, $\epsilon(t)$, is assumed to be a constant.

The internal relative humidity, RH, is related to the water content by the empirical van Genuchten model [13] or derived by the semi-empirical model based on the modified BET adsorption theory [14]. In this model, the theoretic model is used as this RH-water content relationship is expressed with classic adsorption model properties:

$$W_w = \frac{V_m C k \left(\frac{RH}{100}\right)}{\left(1 - k \cdot \frac{RH}{100}\right) [1 + (C-1)k \cdot \frac{RH}{100}]} \tag{13}$$

where W_w is water content by the mass ratio of hardened cement paste (HCP). It should be noted that there were conflicting cited meanings of this parameter in the original reference [11,14], but the above-mentioned one has been verified with the experimental data in that reference. V_m, C, and k are the parameters related to the BET adsorption model and the water-cement ratio of HCP.

$$C = \mathrm{e}^{C_0/T} \tag{14}$$

where C_0 = 855, and T is temperature $[K]$.

The water content $\boldsymbol{W_w}$ can be converted to volumetric water content of HCP by

$$\theta_{w\_HCP} = \frac{1}{1 + \left(\frac{1}{W_w} - 1\right)\rho_w/\rho_c} \tag{15}$$

and further converted to the volumetric water content of concrete, θ_w, by

$$\theta_w = \frac{\theta_{w\_HCP}}{1 + \frac{\frac{a}{c}\frac{\rho_c}{\rho_a}}{1 + \frac{w}{c}\frac{\rho_c}{\rho_w}}} \tag{16}$$

With the relationships among porosity, water content, and oxygen diffusivity established, the influence of temperature on oxygen transport must also be considered. The temperature dependence of the effective oxygen diffusivity can be expressed by an Arrhenius-type equation [11]:

$$D_{e,O_2}(T) = D_{e,O_2,}(T_0) \cdot exp\left[\frac{\Delta U_D}{R}\left(\frac{1}{T_0} - \frac{1}{T}\right)\right] \tag{17}$$

Where T_0 is reference temperature $[K]$, R is the gas constant $[J/K/mol]$, ΔU_D is activation energy $[J]$, and it can be calculated with an empirical expression for water-cement ratio between 0.4 and 0.6:

$$\Delta U_D = 0.001[KJ/J] \cdot \left[-505\left(\frac{w}{c}\right)^2 + 484.5\frac{w}{c} - 94\right] \tag{18}$$

Once the corrosion current density, i_{corr}, is calculated, the corrosion rate or the section loss rate can be calculated with Faraday's laws.

$$r_{corr} = x_{loss\_r} = i_{corr}\frac{M_{Fe}}{nF\rho_{Fe}} \tag{19}$$

where x_{loss_r} is the section loss rate $[m/s]$, M_{Fe} is molar mass $[Kg/mol]$, n is the number of charges, ρ_{Fe} is the density of iron $[Kg/m^3]$.

The distribution of the accumulated rebar section loss at t_{end} accounts for the contributions from all active corrosion events that occur in the time history up to t_{end}.

For an active corrosion event initiated within the interval $[t_i, t_i + \Delta t]$, the corresponding accumulated section loss at t_{end} is

$$\mathrm{x\_loss}_{\mathrm{t_i}\rightarrow t_{end}} = \int_{t_i}^{t_{end}} r_{corr}(t)dt \tag{20}$$

This probability associated with this event is the additional probability of active corrosion onset in $[t_i, t_i + \Delta t]$, expressed as

$$P_{add.onset}(\mathrm{t_i}) = P_{onset}(t_i + \Delta t) - P_{onset}(t_i). \tag{21}$$

The section loss at the time t_{end}, is a random variable constructed with the accumulated section loss from t_i to t_{end} together with the corresponding probability of the corrosion onset event.

1.5 Cracking module

In the scope of the current cracking model, the formed crack is assumed to be corrosion-induced only, with no consideration of other structural stress. The inclusion of other structural stress will be considered in future research projects.

The section loss of the reinforcing steel is derived from the corrosion rate, and the initiation of concrete cover cracking is predicted from the expansive pressure generated by rust accumulation. This rust-induced expansive pressure, acting radially from the rebar onto the surrounding concrete, produces tensile stresses in the direction perpendicular to the principal compressive stresses. The interaction between rust expansion and the concrete cover is represented using the thick-walled cylinder model and its improved formulations [15–17].

The thick-walled cylinder model is based on the following assumptions:

- Smeared cracks propagate through the concrete cover in the radial direction.
- Concrete follows the bilinear tension softening law.
- Radial displacement compatibility exists between cracked and sound
- Three cracking stages are considered: sound, partially cracked, and fully cracked.

The cylinder model is illustrated in Figure 1.

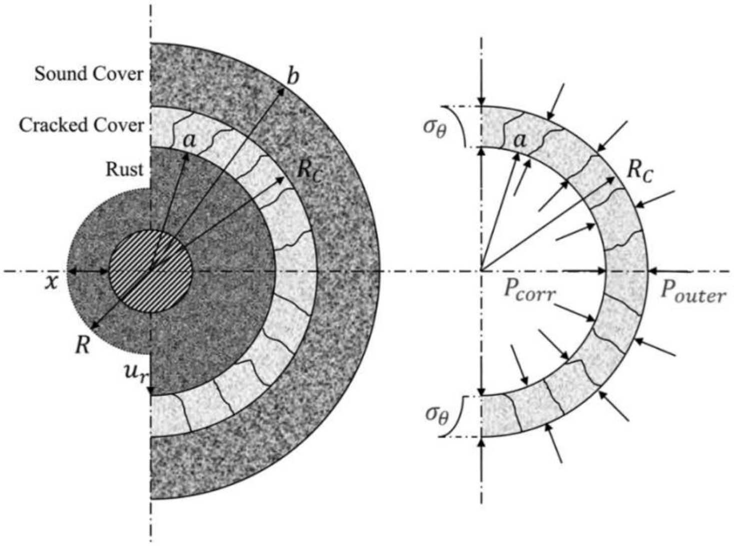

Figure 1 Illustration of the thick-walled cracking model [15]**.**

The tangential strain, ε_θ, in the cylinder can be expressed in terms of the rust thickness.

For sound or fully cracked concrete cover:

$$\varepsilon_\theta(a \le r \le b) = \frac{u_{st}}{a}\frac{\frac{b^2}{r^2}+1}{\frac{b^2}{a^2}+1} \tag{22}$$

For partially cracked concrete cover:

$$\varepsilon_\theta(a \le r \le b) = \frac{f_t}{E_0}\frac{\frac{b^2}{r^2}+1}{\frac{b^2}{R_C^2}+1} \tag{23}$$

with

$$R_C = \frac{b}{\sqrt{\frac{f_t \cdot a}{E_0.u_{st}}\left[\left(\frac{b}{a}\right)^2+1\right]-1}} \tag{24}$$

where,

a: inner radius boundary of the rust (centre of rebar to rust–concrete interface) $[m]$

b : outer radius boundary of the concrete (center of rebar to cover surface) $[m]$

u_{st} : rust expansion depth beyond the ITZ porous zone [m]

f_t : ultimate tensile strength $[MPa]$

E_0 : modulus of elasticity $[MPa]$

R_C: the splitting crack front (center of rebar to concrete where $\sigma_\theta|_{r=R_C} = f_t$)

Taking into account the volumetric expansion rate r_v and the thickness of the porous interfacial transition zone (ITZ) between the rebar and concrete matrix, u_p, the effective rust expansion depth u_{st} can be calculated with the rebar corrosion sectional loss $x(t)$.

$$u_{st} = u_r - u_p \tag{25}$$

$$u_r = (r_v - 1) \cdot x(t) \tag{26}$$

Here, u_r represents the total radial rust growth, i.e., the outward displacement of the rust front due to the volumetric expansion of corrosion products. It is obtained by multiplying the steel section loss, $x(t)$ (expressed as a radial measure), by the expansion factor $(r_v - 1)$. Physically, this means that as the steel radius decreases by $x(t)$, the resulting rust occupies a larger volume, expanding outward and exerting pressure on the surrounding concrete. Subtracting the porous ITZ thickness, u_p, yields the effective expansion u_{st}, which actively contributes to cracking.

The expansion rate r_v ranges from 2 to 6.5 times that of metallic iron, depending on the rust form (Figure 2) [18]. Under field conditions, the rust is typically a mixture of different forms, with a mean expansion rate of $r_v = 2.96$, varying between 2.6 and 3.3 [19,20]. The thickness of the porous zone has a typical value $u_p = 12.5\ \mu m$ [21], and it is affected by the water-cement ratio.

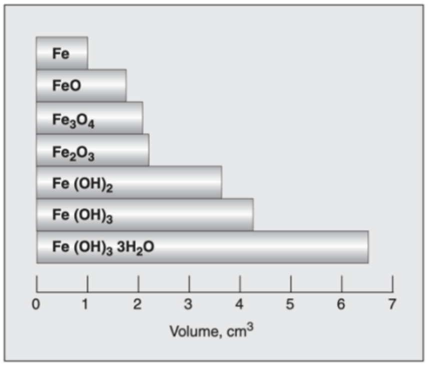

Figure 2 Expansion volume of various rust forms [18]**.**

The tensile stress σ_θ in the concrete cover in the tangential direction is calculated using the bilinear tension-softening constitutive model [22]:

$$\sigma_\theta = \begin{cases} E_0 \cdot \varepsilon_\theta, & \varepsilon_\theta \leq \varepsilon_{cr} \\ f_t \cdot \left[1 - 0.85 \cdot \dfrac{\varepsilon_\theta - \varepsilon_{cr}}{\varepsilon_1 - \varepsilon_{cr}}\right], & \varepsilon_{cr} \leq \varepsilon_\theta \leq \varepsilon_1 \\ 0.15 \cdot f_t \cdot \dfrac{\varepsilon_u - \varepsilon_\theta}{\varepsilon_u - \varepsilon_1}, & \epsilon_1 \leq \epsilon_\theta \leq \epsilon_u \end{cases} \tag{27}$$

where

$\varepsilon_{cr} = f_t/E_0$ is the critical cracking strain

ε_1 = 0.0003 is the strain corresponding to $\sigma_\theta = 0.15f_t$

ε_u = 0.002 is the ultimate strain corresponding to zero residual tensile strength

The model is depicted in Figure 3.

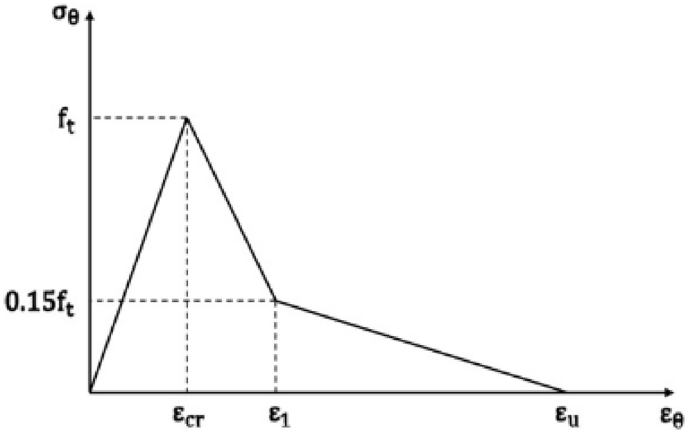

Figure 3 Bilinear tension-softening constitutive model [22].

As smeared cracks propagate through the concrete cover in the partially cracked condition, the first single crack appears as a crack through the concrete cover, which leads to the fully cracked condition. The crack width of the discrete open crack is calculated by integrating the tensile strain that exceeds the critical cracking strain [23] when the crack tip reaches the concrete cover surface:

$$w_{open} = \int_0^{2\pi b} (\varepsilon_\theta|_{r=b} - \varepsilon_{cr}) ds = 2\pi b \left[\frac{2}{\left(\frac{b}{a}\right)^2 + 1} \cdot \frac{u_{st}}{a} - \varepsilon_{cr} \right] \tag{28}$$

Here, w_{open} represents the circumferential crack opening width at the concrete cover surface.

This cracking module calculates the distribution of the internal cracks and the probability of surface cracking. For each stochastic sample calculation, after evaluating $\varepsilon_\theta(r)$ on a radial grid $r \in [a, b]$, the cover condition is classified as

- Sound cover: $\varepsilon_\theta(r) < \varepsilon_{cr}$ for all $r \in [a, b]$.
- Partially cracked: there exist $r_1, r_2 \in [a, b]$ such that $\varepsilon_\theta(r_1) \geq \varepsilon_{cr}$ and $\varepsilon_\theta(r_2) \leq \varepsilon_{cr}$.
- Fully cracked: $\varepsilon_\theta(r) \geq \varepsilon_{cr}$ for all $r \in [a, b]$.

For partially cracked states, the crack-front radius R_C is computed from Equation (24). For fully cracked states, $R_C = b$. For sound states, no discrete crack forms (R_C is undefined).

The probability of surface cracking is the probability of the fully cracked condition, which is equivalently the probability that the crack front reaches the cover surface:

$$P_{\text{surface cracking}} = \mathrm{P}\,(R_C = b) \tag{29}$$

The internal crack length is reported via the normalised crack length (crack-length–over–cover). Let R denote the original rebar radius and cover $= b - R$:

$$\Lambda = \frac{L_{\text{crack}}}{\text{cover}} = \frac{R_C - \mathrm{R}}{\mathrm{b} - \mathrm{R}} \tag{30}$$

The distribution of internal crack length is the distribution of Λ across all stochastic samples.

Note: Detailed implementation procedures are provided in the Rational-RC software package documentation [6].

2 Rational-RC computer code implementation

Rational-RC adopts a modular, object-oriented architecture, enabling deterioration models to be updated or extended independently without disrupting the overall framework [6]. The package includes five main modules (.py files) as outlined below.

- **`membrane.py`**: Models the probability of failure in waterproof membranes, using a statistical approach that accounts for service life variability.
- **`chloride.py`**: Simulates chloride penetration into concrete through diffusion-advection mechanisms and calibrates based on field data.
- **`carbonation.py`**: Predicts carbonation depth overtime considering environmental factors and material properties.
- **`corrosion.py`**: Estimates uniform corrosion of rebar using a combination of empirical and electrochemical models, considering factors such as water content, temperature, and oxygen availability.
- **`cracking.py`**: Evaluates the probability of cracking due to rust expansion, utilizing a thick-walled cylinder model to predict crack initiation and propagation in the concrete cover.

The main modules are implemented in a similar structure to ensure consistency. The software architecture of these main modules can be represented by the following high-level structure (Figure 4).

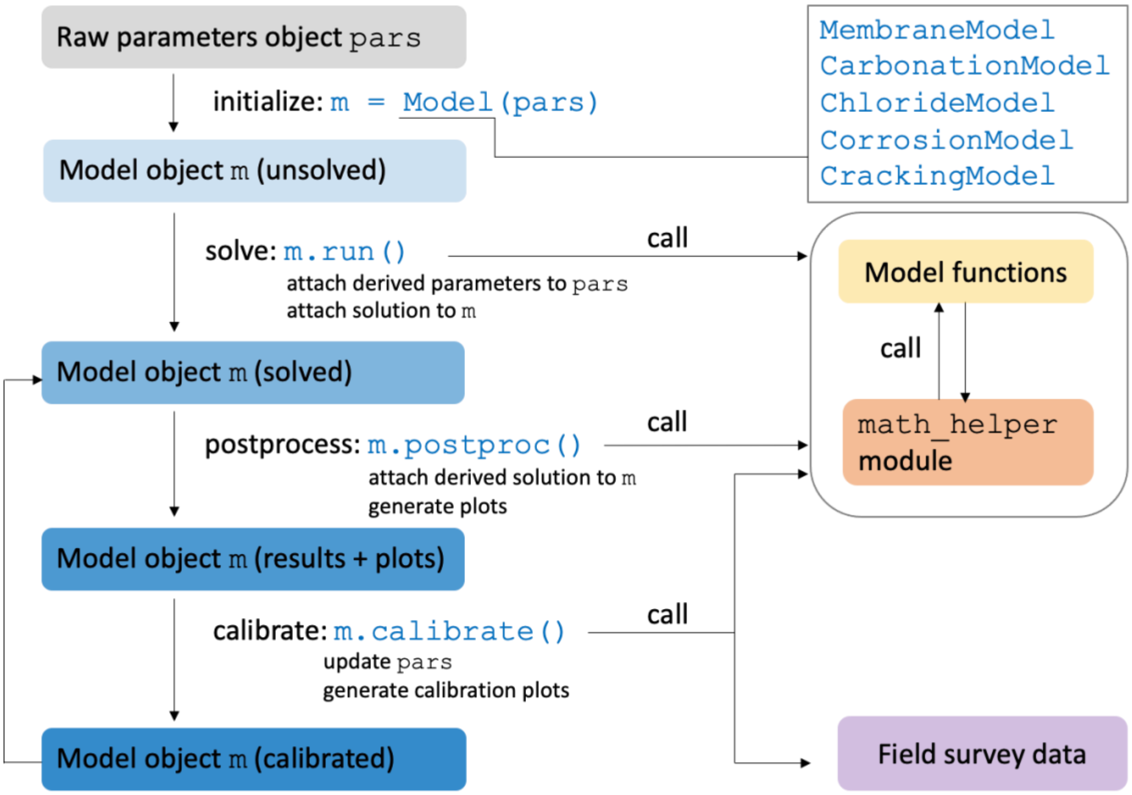

Figure 4 High-level architecture of the main deterioration modules in rational-rc [6]**.**

In each main module, raw parameters such as material properties and exposure conditions are assigned as attributes to the parameter object, `pars`. The model object, `m`, is then initialized using `pars`. This object, `m`, holds all the raw data (`m.pars`) along with methods and model functions related to the specific deterioration mechanism in that module. The `m.run()` method performs the calculations, updates intermediate parameters in `m.pars`, and attaches the direct solution to `m`. The `m.postproc()` method post-processes these direct results, generating derived outputs such as the probability of failure, beta factor, and visualizations. The `m.calibrate()` method calibrates the model by adjusting the material properties to match field data, returning a deep-copied new calibrated model object while preserving the original model (`m`).

During the execution of `run()`, `postproc()`, and `calibrate()`, the `math_helper` module is invoked to handle shared utility tasks such as distribution sampling for random variability, probability parameter fitting, and generating visualizations. This architecture ensures modularity and interaction between the main modules and the `math_helper` module.

Rational-RC employs modular Monte Carlo simulation with efficient vectorized operations and is architected to support scalable execution through user-defined parallel processing. A complete four-stage deterioration simulation (membrane aging, chloride ingress, corrosion, and cracking) using 10^5 samples typically completes in under 5 minutes on a standard laptop (Intel i9 processor, 16 GB RAM), making it well-suited for element-level and small-to-medium-scale applications. Basic tutorials for each module are available on the documentation website under Tutorials.

3 Reference

[1] G. Li, J. Zacaruk, M. Boulfiza, Rational-RC: A Practical Life Cycle Deterioration Modelling Framework for Reinforced Concrete Structures, (2022). https://rational-rc.readthedocs.io/en/latest/ (accessed April 29, 2025).

[2] Geoffrey. Mays, Durability of concrete structures : investigation, repair, protection, in: Taylor & Francis, 2004.

[3] U. Angst, B. Elsener, C.K. Larsen, Ø. Vennesland, Critical chloride content in reinforced concrete — A review, Cem Concr Res 39 (2009) 1122–1138. https://doi.org/10.1016/j.cemconres.2009.08.006.

[4] R.B. Figueira, A. Sadovski, A.P. Melo, E. V Pereira, Chloride threshold value to initiate reinforcement corrosion in simulated concrete pore solutions: The influence of surface finishing and pH, Constr Build Mater 141 (2017) 183–200. https://doi.org/10.1016/j.conbuildmat.2017.03.004.

[5] P. Schiessl, S. Helland, C. Gehlen, L.O. Nilsson, S. Rostam, fib bulletin 34 - Model code for service life design (MC-SLD), fib. The International Federation for Structural Concrete, 2005. https://doi.org/10.35789/fib.BULL.0034.

[6] G. Li, J. Zacaruk, M. Boulfiza, Rational-RC: A Python package for probabilistic life-cycle deterioration modelling of reinforced concrete structures, SoftwareX 31 (2025). https://doi.org/10.1016/j.softx.2025.102238.

[7] A. V Saetta, B.A. Schrefler, R. V Vitaliani, The Carbonation of Concrete and the Mechanism of Moiture, Heat and Carbon Dioxide Flow Through Porous Materials, Cem Concr Res 23 (1993) 761–772.

[8] O.B. Isgor, a. G. Razaqpur, Finite element modeling of coupled heat transfer, moisture transport and carbonation processes in concrete structures, Cem Concr Compos 26 (2004) 57–73. https://doi.org/10.1016/S0958-9465(02)00125-7.

[9] M. Pour-Ghaz, O.B. Isgor, P. Ghods, The effect of temperature on the corrosion of steel in concrete. Part 1: Simulated polarization resistance tests and model development, Corros Sci 51 (2009) 415–425. https://doi.org/10.1016/j.corsci.2008.10.034.

[10] B. Yu, J. Liu, B. Li, Improved numerical model for steel reinforcement corrosion in concrete considering influences of temperature and relative humidity, Constr Build Mater 142 (2017) 175–186. https://doi.org/10.1016/j.conbuildmat.2017.03.045.

[11] M. Pour-Ghaz, O. Burkan Isgor, P. Ghods, The effect of temperature on the corrosion of steel in concrete. Part 2: Model verification and parametric study, Corros Sci 51 (2009) 426–433. https://doi.org/10.1016/j.corsci.2008.10.036.

[12] V.G. Papadakis, C.G. Vayenas, M.N. Fardis, Physical,and Chemical Characteristics Affecting the Durability of Concrete, ACI Mater J 88 (1991) 186–196.

[13] M.T. Van Genuchten, A closed-form equation for predicting the hydraulic conductivity of unsaturated soils 1, Soil Science Society of America Journal 44 (1980) 892–898.

[14] Y. Xi, Z.P. Bažant, H.M. Jennings, Moisture diffusion in cementitious materials Adsorption isotherms, Advanced Cement Based Materials 1 (1994) 248–257. https://doi.org/10.1016/1065-7355(94)90033-7.

[15] C. Cao, M.M.S. Cheung, B.Y.B. Chan, Modelling of interaction between corrosion-induced concrete cover crack and steel corrosion rate, Corros Sci 69 (2013) 97–109. https://doi.org/10.1016/j.corsci.2012.11.028.

[16] I. Balafas, C.J. Burgoyne, Modeling the Structural Effects of Rust in Concrete Cover, J Eng Mech 137 (2011) 175–185. https://doi.org/10.1061/(ASCE)EM.1943-7889.0000215.

[17] X. Wang, X. Liu, Bond strength modeling for corroded reinforcements, Constr Build Mater 20 (2006) 177–186. https://doi.org/10.1016/j.conbuildmat.2005.01.015.

[18] P.K. Mehta, P.J.M. Monteiro, Concrete : microstructure, properties, and materials., Third Edit, McGraw-Hill, 2006. https://doi.org/10.1036/0071462899.

[19] K. Suda, S. Misra, K. Motohashi, CORROSION PRODUCTS OF REINFORCING BARS EMBEDDED IN CONCRETE, 1993.

[20] Y. Zhao, H. Ren, H. Dai, W. Jin, Composition and expansion coefficient of rust based on X-ray diffraction and thermal analysis, Corros Sci 53 (2011) 1646–1658. https://doi.org/10.1016/j.corsci.2011.01.007.

[21] Youping Liu and Richard Weyers, Modeling the Time-to-Corrosion Cracking in Chloride Contaminated Reinforced Concrete Structures, ACI Mater J 95 (1998) 675–680. https://doi.org/10.14359/410.

[22] X.H. Wang, X.L. Liu, Modelling effects of corrosion on cover cracking and bond in reinforced concrete, Magazine of Concrete Research 56 (2004) 191–199. https://doi.org/10.1680/macr.2004.56.4.191.

[23] H.M. Shodja, K. Kiani, A. Hashemian, A model for the evolution of concrete deterioration due to reinforcement corrosion, Math Comput Model 52 (2010) 1403–1422. https://doi.org/10.1016/j.mcm.2010.05.023.